Introduction to the Edge Equilibrium Code (EEC)*

Xujing Li

Institute of Computational Mathematics and Scientific/Engineering Computing,
Academy of Mathematics and Systems Science, Chinese Academy of Sciences,

At present, 2 years visiting scientist at PPPL

PPPL Theory Seminar,

May 30, 2013, PPPL, Princeton NJ

*This work is partially supported by US DoE contract No. DE-AC02-09-CH11466,
by the National Magnetic Confinement Fusion Science Program 2011GB105003,
and by the US DOE SBIR grant # 94307S10-II

PPPL PRINCETON PLASMA PHYSICS LABORATORY

Abstract

The talk presents the Edge Equilibrium Code (EEC), which is a new solver of the Grad-Shafranov equation complementing the existing ESC code (based on Fourier representation). EEC, being developed specifically for the near edge region with an arbitrary shape of the plasma boundary, uses adaptive flux coordinates with Hermite finite element representation. A special routine for fast solving the sparse matrix equations was created for EEC.

The edge solution of EEC is matched with the core solution from ESC through a virtual boundary and the two codes communicate as two parallel processes. This approach addresses the future needs in enhancing functionality of EEC without conflicting with the interface of both codes. The CodeBuilder (Cb), which maintains the documentation and the source code consistent with each other, was used for the code development.

The resulting ESC-EEC code system acquired unmatched ability (a) in fast free and fixed boundary equilibrium calculations for arbitrary plasma shapes, (b) in using both $r - z$ and different flux coordinates, (c) in choosing different combinations of input profiles, (d) in performing equilibrium reconstruction together with variances analysis, and (e) in assessing the diagnostics used for equilibrium reconstruction.

Contents

1 Introduction to equilibrium problems

Looking as a very primitive problem, the tokamak equilibrium is absolutely essential for magnetic fusion by giving the background information about magnetic configuration.

For tokamaks Grad-Shafranov (GSh) equation

$$\Delta^*\bar{\Psi} = -r^2 P(\bar{\Psi}) - T(\vec{\Psi}), \quad \bar{\Psi} \equiv \frac{\Psi}{2\pi}, \quad P \equiv \frac{d\mu_0 p}{d\bar{\Psi}}, \quad T \equiv \bar{F}\frac{d\bar{F}}{d\bar{\Psi}}, \quad \bar{F} \equiv rB_{tor} \qquad (1.1)$$

describes well the real plasma, rather than its theoretical models.

The use of flux coordinates a, θ ($\bar{\Psi} = \bar{\Psi}(a)$) is critical for high temperature plasma. Laboratory r, z or other u, v coordinates cannot provide the necessary accuracy.

The practical problems for tokamak equilibria can be listed as

	a, θ	r, z or laboratory u, v
Fixed simple boundary, P, T as the RHS	perfect	not accurate
Fixed simple boundary, arbitrary RHS	perfect	bad
Fixed boundary with X-points	problematic	not accurate
Free boundary	problematic	good for plasma control
Equilibrium reconstruction	problematic	limited justification
Variances analysis	perfect (ESC)	not performed
Real time forecast of plasma discharge	perfect (ESC)	not suitable

ESC and its capacities

ESC is the only existing code addressing all listed problems

Solves the linearized GSh equation

$$\bar{\Psi} = \bar{\Psi}_0 + \tilde{\psi}, \quad \Delta^*\bar{\Psi} + r^2\frac{dP}{d\bar{\Psi}_0}\tilde{\psi} + \frac{dT}{d\bar{\Psi}_0}\tilde{\psi} = -r^2P - T \qquad (1.2)$$

by special shooting technique. Used a simple Fourier representation

$$r = r_0 + \sum r_m e^{im\theta}, \quad z = z_0 - b\sin\theta, \quad \bar{\Psi} = \bar{\Psi}_0 + \sum \bar{\Psi}_m e^{im\theta}. \qquad (1.3)$$

Automatically provides information about linearized axisymmetric perturbations necessary for vertical stability analysis.

	a, θ
Fixed simple boundary *Fixed simple boundary, arbitrary RHS* *Fixed boundary with X-points* *Free boundary*	*6 choices of* a $\simeq 20$ *combinations of plasma profiles* *analytical BL* *interacting* a, θ *and* r, z *solvers* *X-points ignored in* a, θ *solver*
Equilibrium reconstruction *First reconstructions* *Variances analysis*	$\bar{\Psi}_i, B_i$*, MSE-LP, MSE-LS, Faraday rotation* *transport profiles as signals* *Plasma with the current holes (JET)* *Response function technique (CDX-U)* *Unique*
Real time forecast of plasma discharge needed for EAST	*ESC-ASTRA is the prototype of RTF (fast equilibrium at every time step)*

Needs in EEC

For the separatrix limited plasma ESC incorporates a virtual boundary, separating the core and the boundary layer.

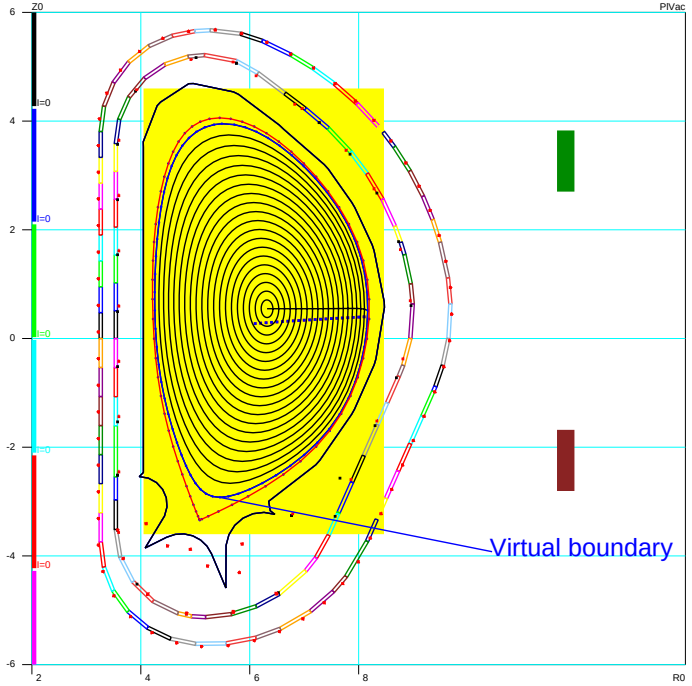

ITER equilibrium

For the core: Fourier representation of $r(a,\theta), z(a,\theta), \bar{\Psi}(a,\theta)$.

For the edge: analytical model.

At the virtual boundary: $\bar{\Psi}, B_{pol}$ ***are continuous.***

The objective of EEC: the replacement of analytical model by a finite element solution

EEC has to be able to solve the GSh equation for arbitrary mixture of Dirichlet and Neumann boundary conditions. Physics needs Neumann boundary conditions.

The next steps will involve linking ESC-EEC with the plasma surface current and shell codes for simulation of Hiro currents and vertical disruptions in tokamaks.

2 Edge Equilibrium Code

The tokamak Grad-Shafranov (GSh) equilibrium equation

$$\Delta^*\bar{\Psi} \equiv r\frac{\partial}{\partial r}\left(\frac{1}{r}\frac{\partial\bar{\Psi}}{\partial r}\right)+\frac{\partial^2\bar{\Psi}}{\partial z^2}=-r^2\frac{d\bar{p}}{d\bar{\Psi}}-\bar{F}\frac{d\bar{F}}{d\bar{\Psi}} \tag{2.1}$$

can be obtained from the energy principle

$$W=\frac{1}{2}\int\left\{\frac{|\nabla\bar{\Psi}|^2}{r^2}-2\bar{p}(\bar{\Psi})-\frac{\bar{F}^2(\bar{\Psi})}{r^2}\right\}dxdydz. \tag{2.2}$$

In toroidal coordinates a,θ,ϕ

$$r=r(a,\theta),\quad z=z(a,\theta),\quad D\equiv\frac{D(r,z)}{D(a,\theta)},\quad \bar{\Psi}=\bar{\Psi}(a,\theta), \tag{2.3}$$

the W ***functional has the form***

$$W=\frac{1}{2}\int\left\{\frac{g_{\theta\theta}}{rD}\bar{\Psi}_a'^2-2\frac{g_{a\theta}}{rD}\bar{\Psi}_a'\bar{\Psi}_\theta'+\frac{g_{aa}}{rD}\bar{\Psi}_\theta'^2-2rD\bar{p}(\bar{\Psi})-\frac{D}{r}\bar{F}^2(\bar{\Psi})\right\}dad\theta, \tag{2.4}$$

which can be used for finite element numerical schemes.

2.1 Hermite finite elements

Physics needs knowledge of functions and their first derivatives.

This naturally determines the use of Hermite finite elements on the grid a, θ:

1. ***Values of $\bar{\Psi}$ and its first derivatives $\bar{\Psi}'_a$, $\bar{\Psi}'_\theta$ (together with $\bar{\Psi}''_{a\theta}$) in vertices are obtained explicitly as the solution of discrete equations;***
2. ***Smooth continuous representation of the solution is provided (necessary for grid-less interfaces);***
3. ***Simplicity of interconnection with neighboring elements on rectangular a, θ grids, resulting in well structured tri-diagonal matrix equations.***

$$\bar{\Psi} = \sum_{j=0}^{j<16} V^j(a,\theta) Y_j, \quad \bar{\Psi}'_a = \sum_{j=0}^{j<16} V'^j_a Y_j, \quad \bar{\Psi}'_\theta = \sum_{j=0}^{j<16} V'^j_\theta Y_j \tag{2.5}$$

where $V^j(a,\theta)$ are bicubic spline basis functions, and

$$\begin{aligned}\vec{Y} = \{ & \bar{\Psi}_{00}, \bar{\Psi}'_{a00}, \bar{\Psi}'_{\theta 00}, \bar{\Psi}''_{a\theta 00}, \quad \bar{\Psi}_{10}, \bar{\Psi}'_{a10}, \bar{\Psi}'_{\theta 10}, \bar{\Psi}''_{a\theta 10}, \\ & \bar{\Psi}_{11}, \bar{\Psi}'_{a11}, \bar{\Psi}'_{\theta 11}, \bar{\Psi}''_{a\theta 11}, \quad \bar{\Psi}_{01}, \bar{\Psi}'_{a01}, \bar{\Psi}'_{\theta 01}, \bar{\Psi}''_{a\theta 01} \}\end{aligned} \tag{2.6}$$

2.2 Adaptive grid of EEC

The initial grid for EEC is typically taken from ESC with modification of $\theta = const$ lines by straight lines.

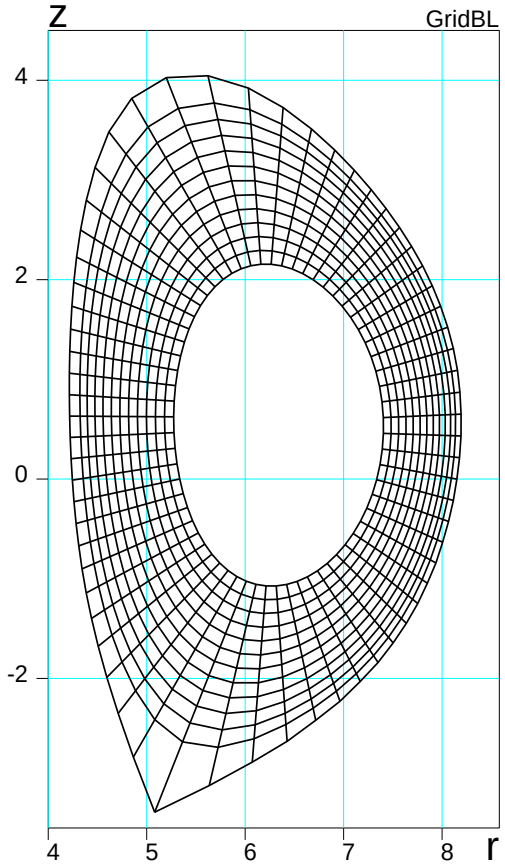

Grid in a "thick" boundary layer

The coordinates a, θ are introduced through Hermite finite elements as well

$$\vec{r} \equiv \{r, z\}, \quad \vec{r} = \sum_{j=0}^{j<16} V^j(a,\theta)\vec{R}_j,$$
$$\vec{r}'_a = \sum_{j=0}^{j<16} V'^j_a \vec{R}_j, \quad \vec{r}'_\theta = \sum_{j=0}^{j<16} V'^j_\theta \vec{R}_j \qquad (2.7)$$

where

$$\vec{R}^T = \{\vec{r}_{00}, \vec{r}'_{a00}, \vec{r}'_{\theta 00}, \vec{r}''_{a\theta 00}, \quad \vec{r}_{10}, \vec{r}'_{a10}, \vec{r}'_{\theta 10}, \vec{r}''_{a\theta 10},$$
$$\vec{r}_{11}, \vec{r}'_{a11}, \vec{r}'_{\theta 11}, \vec{r}''_{a\theta 11}, \quad \vec{r}_{01}, \vec{r}'_{a01}, \vec{r}'_{\theta 01}, \vec{r}''_{a\theta 01}\} \qquad (2.8)$$

This provides consistency in approximations of r, z and $\bar{\Psi}$

The grid adaptation toward $\bar{\Psi} = const$ surfaces is implemented as a Newton scheme

$$\bar{\Psi}(a,\theta) \equiv \bar{\Psi}_0(a) + \tilde{\psi}, \quad \xi = -\frac{\tilde{\psi}}{\bar{\Psi}'_0}, \quad r \to r + r'_a\xi + r'_\theta\sigma, \quad z \to z + z'_a\xi + z'_\theta\sigma, \qquad (2.9)$$

where σ provides straight lines of $\theta = const$.

2.3 Block tri-diagonal matrix

For both 2- and 3-D cases, the matrix resulting from W can be reduced to a block-tri-diagonal cycle matrix by appropriate enumeration.

2-D structure of the matrices

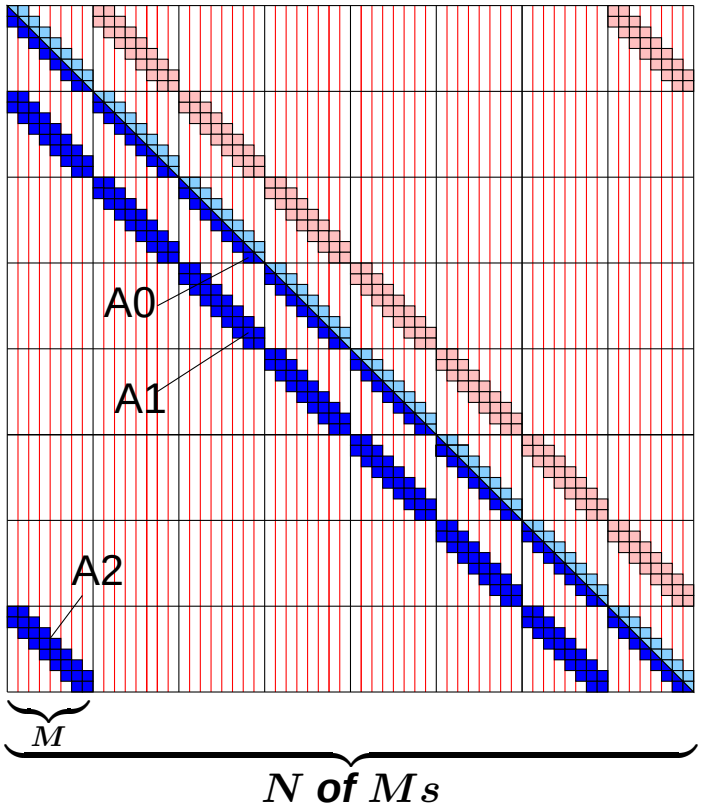

1. ***The elementary tokens for 2-D case are 4x4 matrices. For 3-D case with $\bar{\Psi}, \bar{\Phi}$ unknown, they would be (2x8)x(2x8) matrices;***
2. ***Then, these tokens compose a tri-diagonal $M \times M$ matrices, with M equal to the number of radial a vertexes;***
3. ***Then, these radial matrices compose a periodic tri-diagonal $N \times N$ matrix, corresponding to the poloidal coordinate θ.***
4. ***In the 3-D case, these poloidal matrices would compose a periodic tri-diagonal $L \times L$ matrix, corresponding to the toroidal angle ϕ.***

Block-tri-diagonal algorithm was implemented as a first solver of matrix equation. It works well.

Still, the tri-diagonal structure of elementary matrices is lost in the process of their inversion.

2.4 Cholesky decomposition scheme

Fast Cholesky decomposition scheme was developed to utilize the special structure of the matrix

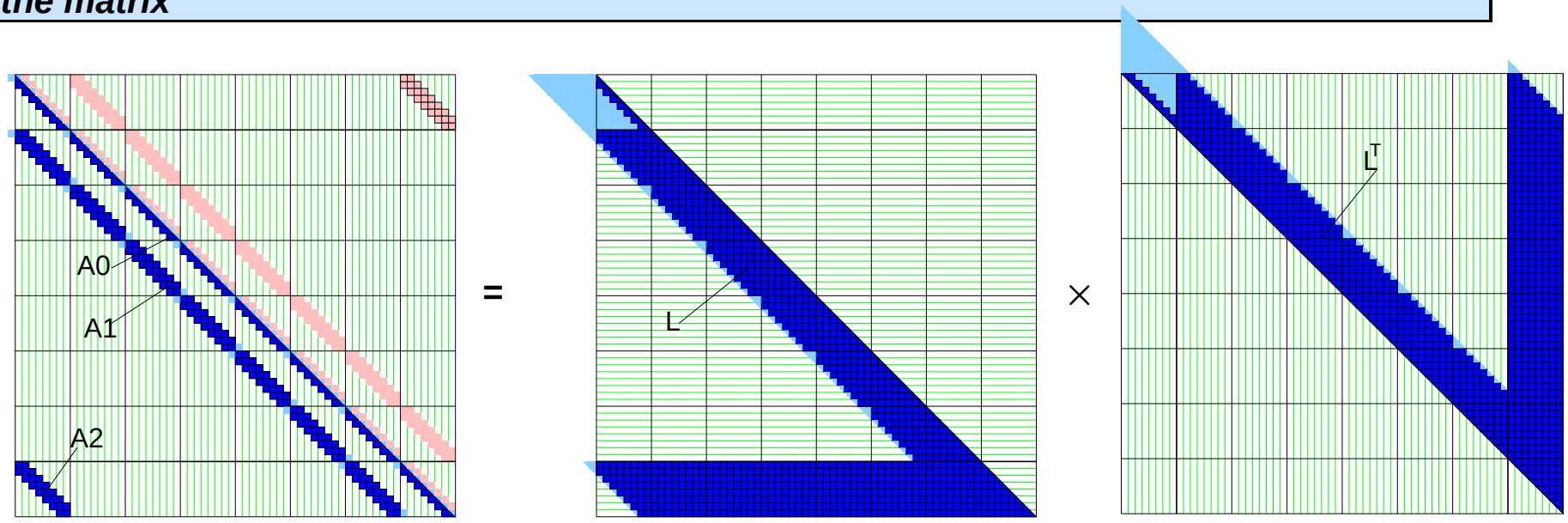

The block-band structure of Cholesky matrices. Light blues represent zeros

After decomposition the resulting band matrices can be used for many RHS of equations.

Use of the CodeBuilder was critical for the development of an efficient Cholesky routine, which has a sophisticated logic of pointers.

2.5 Verification using exact solutions

Numerical solution was tested against analytical solutions of the GSh operator

$$\Delta^* \bar{\Psi} = -r\bar{j}$$

with different combinations of Dirichlet and Neumann boundary conditions

Exact polynomial homogeneous solutions to the GSh equation were generated as

$$Y''_{rr} - \frac{1}{r}Y'_r + Y''_{zz} = r\left(\frac{Y'_r}{r}\right)'_r + Y''_{zz} = 0,$$

$$Y^m_{even} = \sum_{k=0}^{k<m} c_k r^{2(m-k)} z^{2k}, \quad c_{k+1} = -c_k \frac{2(m-k)(m-k-1)}{(k+1)(2k+1)}, \tag{2.10}$$

$$Y^{m+1}_{odd} = \sum_{k=0}^{k<m} s_k r^{2(m-k)} z^{2k+1}, \quad s_{k+1} = -s_k \frac{2(m-k)(m-k-1)}{(k+1)(2k+3)}.$$

Similarly, the polynomial solutions were generated with a polynomial RHS.

Test examples with different $\bar{j} \neq 0$

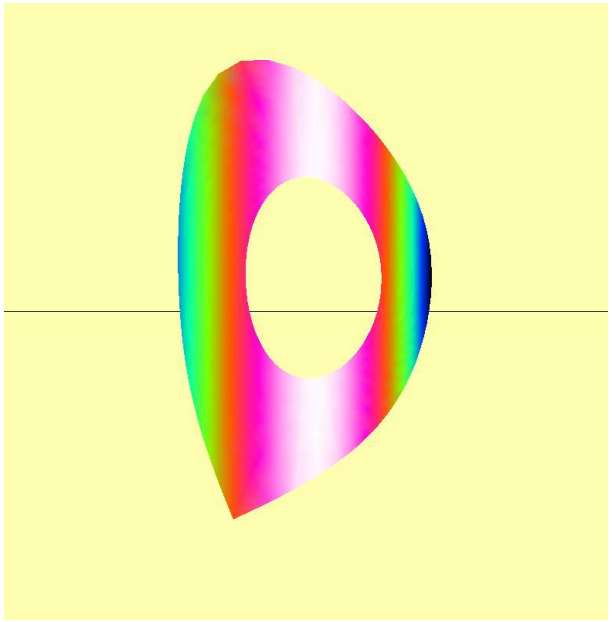

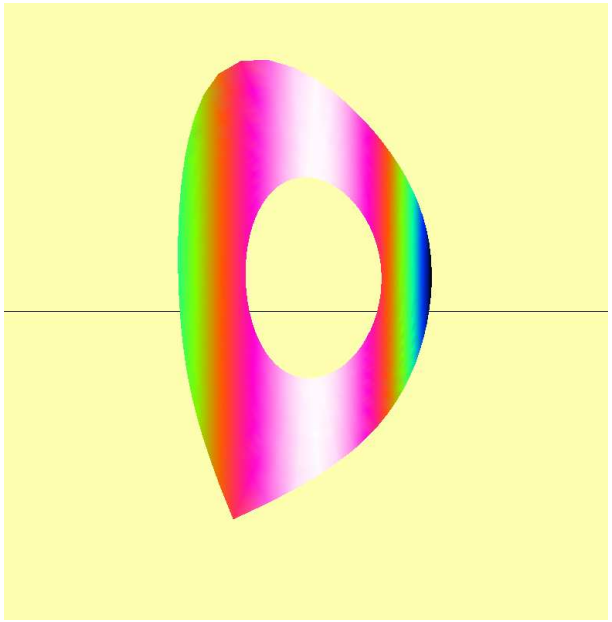

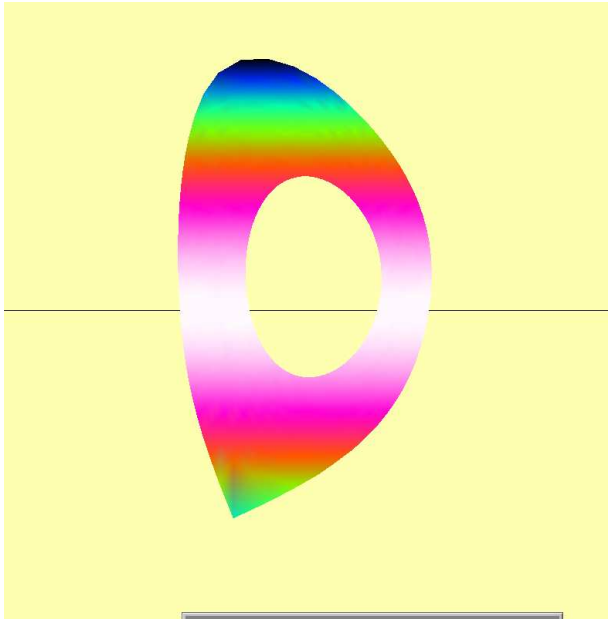

OpenGL color graphics was used for debugging and verification of EEC

With $M \times N = 12 \times 64$ grid covering 0.5 of the minor radius the accuracy 10^{-5} was typical for all combinations of boundary conditions.

Typical homogeneous solutions, $\bar{j} = 0$

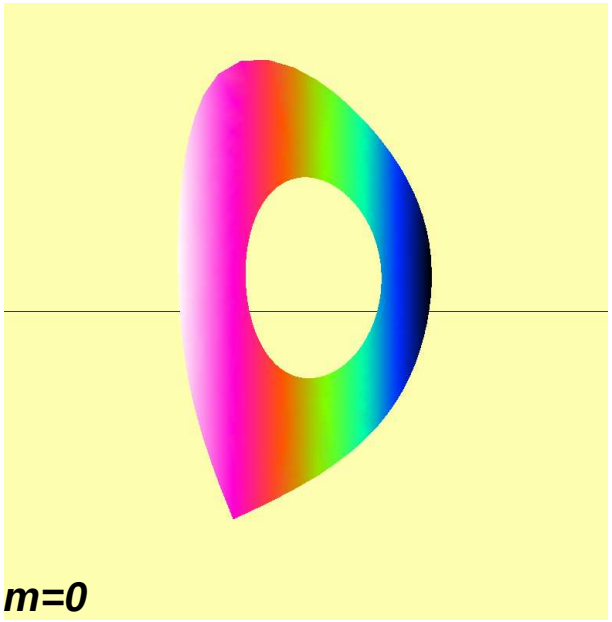

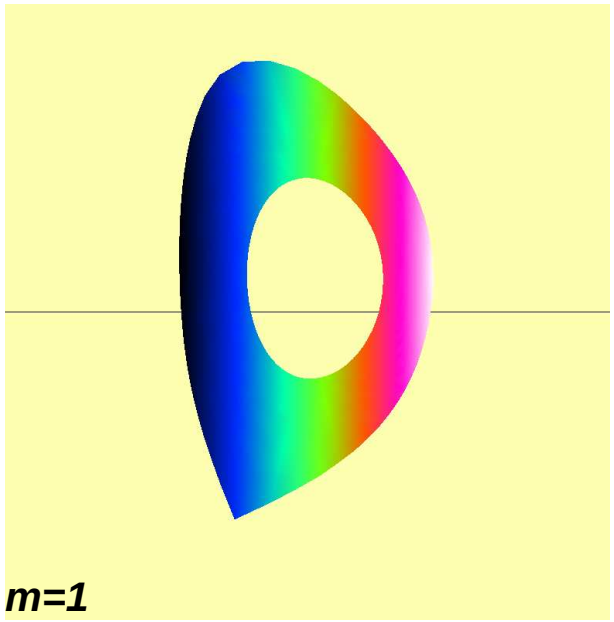

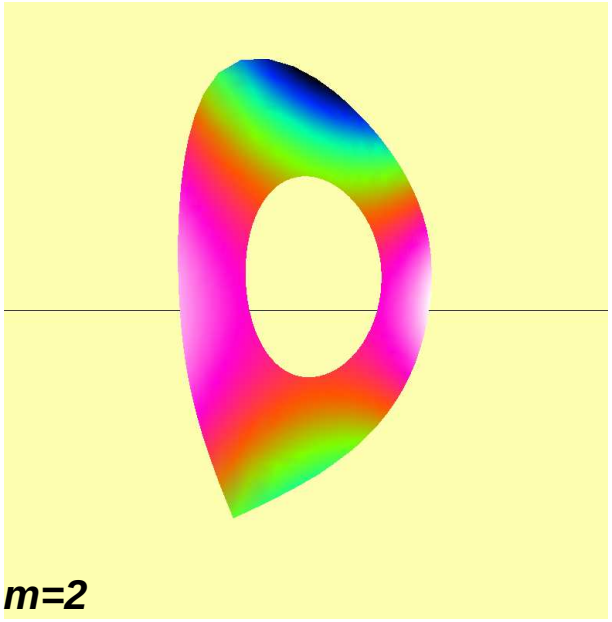

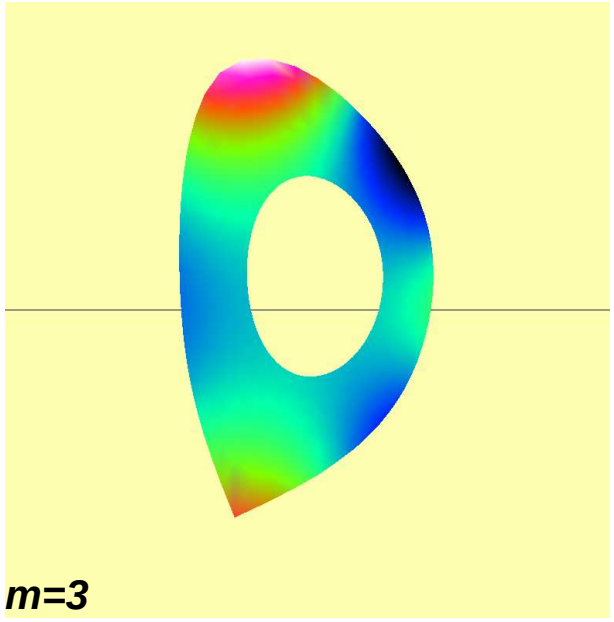

2.6 Examples of EAST equilibria

Conventional tokamak configuration: $R = 2$ m, $a = 0.5$ m

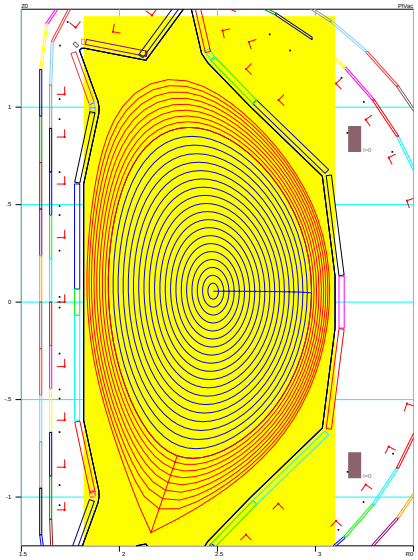

$\beta = 0.5\%$

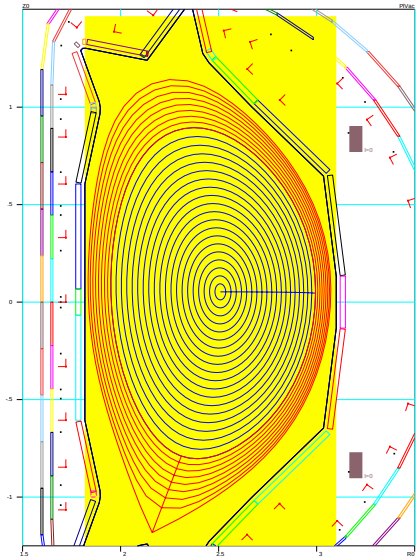

$\beta = 1\%$

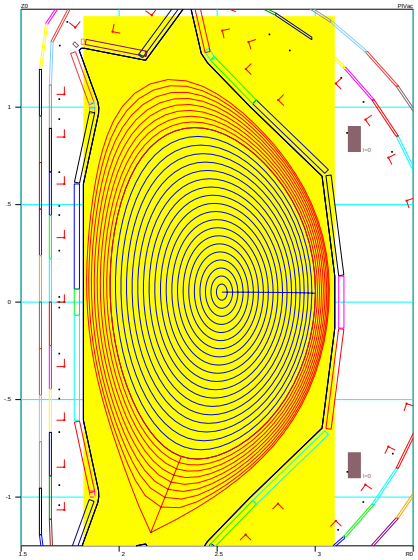

$\beta = 2\%$

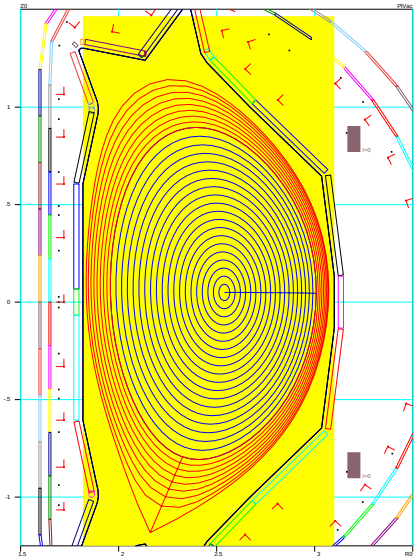

$\beta = 2.5\%$

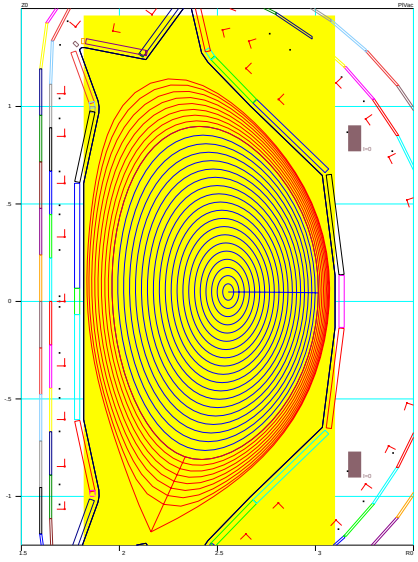

$\beta = 3\%$

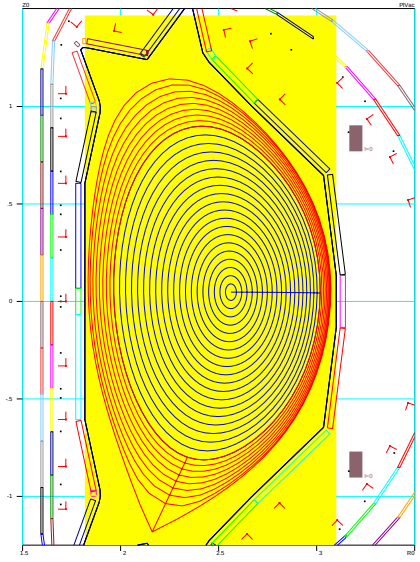

$\beta = 3.5\%$

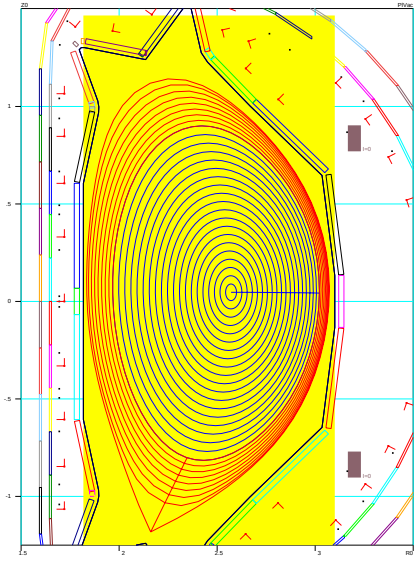

$\beta = 4\%$

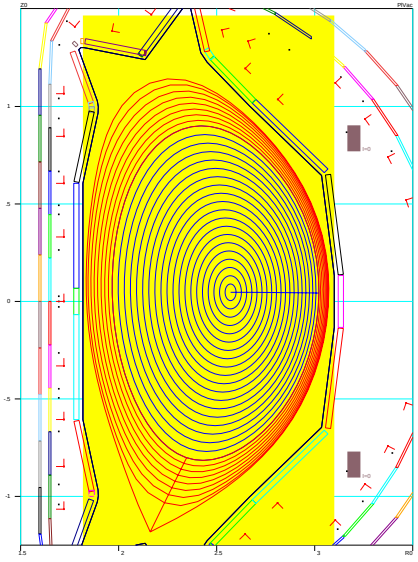

$\beta = 5\%$

2.7 Examples of NSTX equilibria

Small aspect ratio tokamak configuration: $R = 0.88$ ***m,*** $a = 0.65$ ***m***

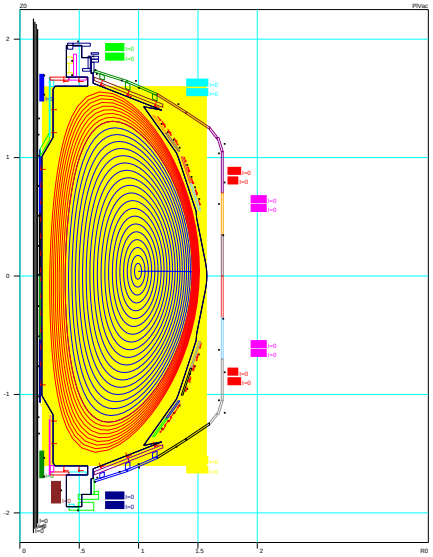

$\beta = 4\%$

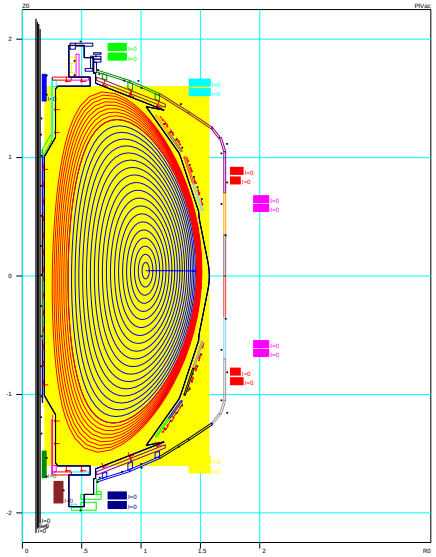

$\beta = 8\%$

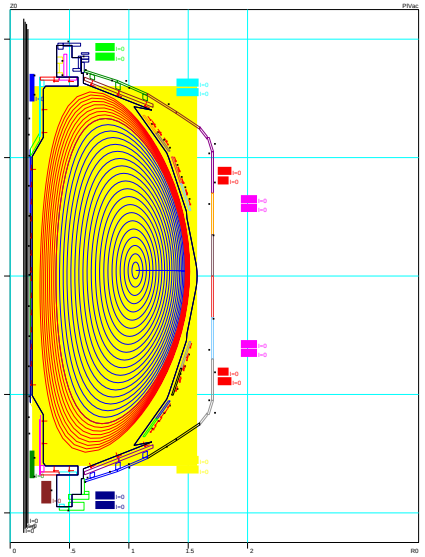

$\beta = 12\%$

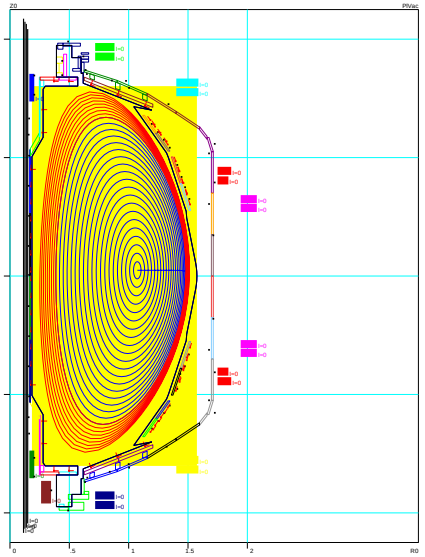

$\beta = 16\%$

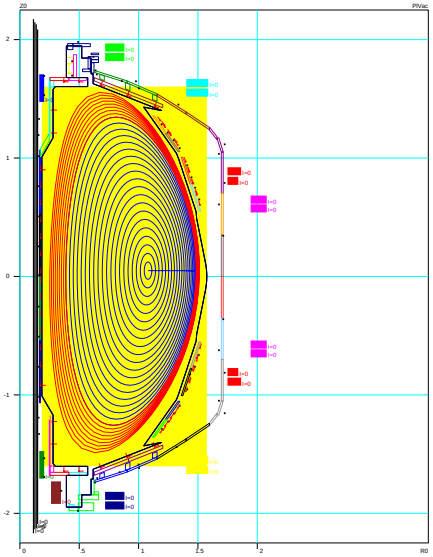

$\beta = 20\%$

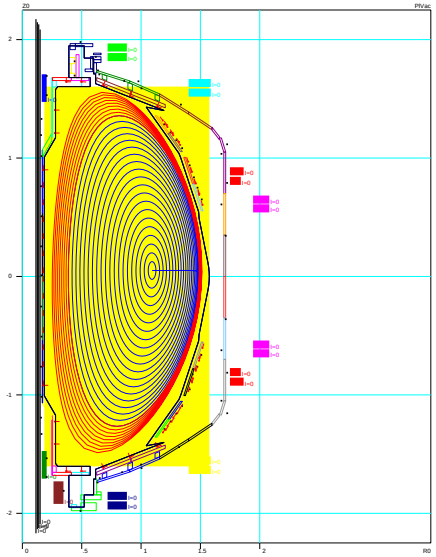

$\beta = 24\%$

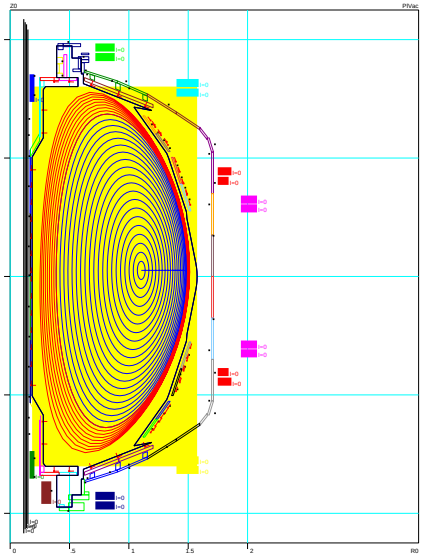

$\beta = 29\%$

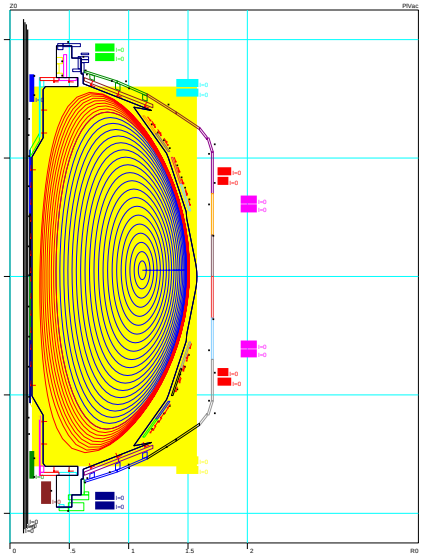

$\beta = 35\%$

High-beta, bigger view

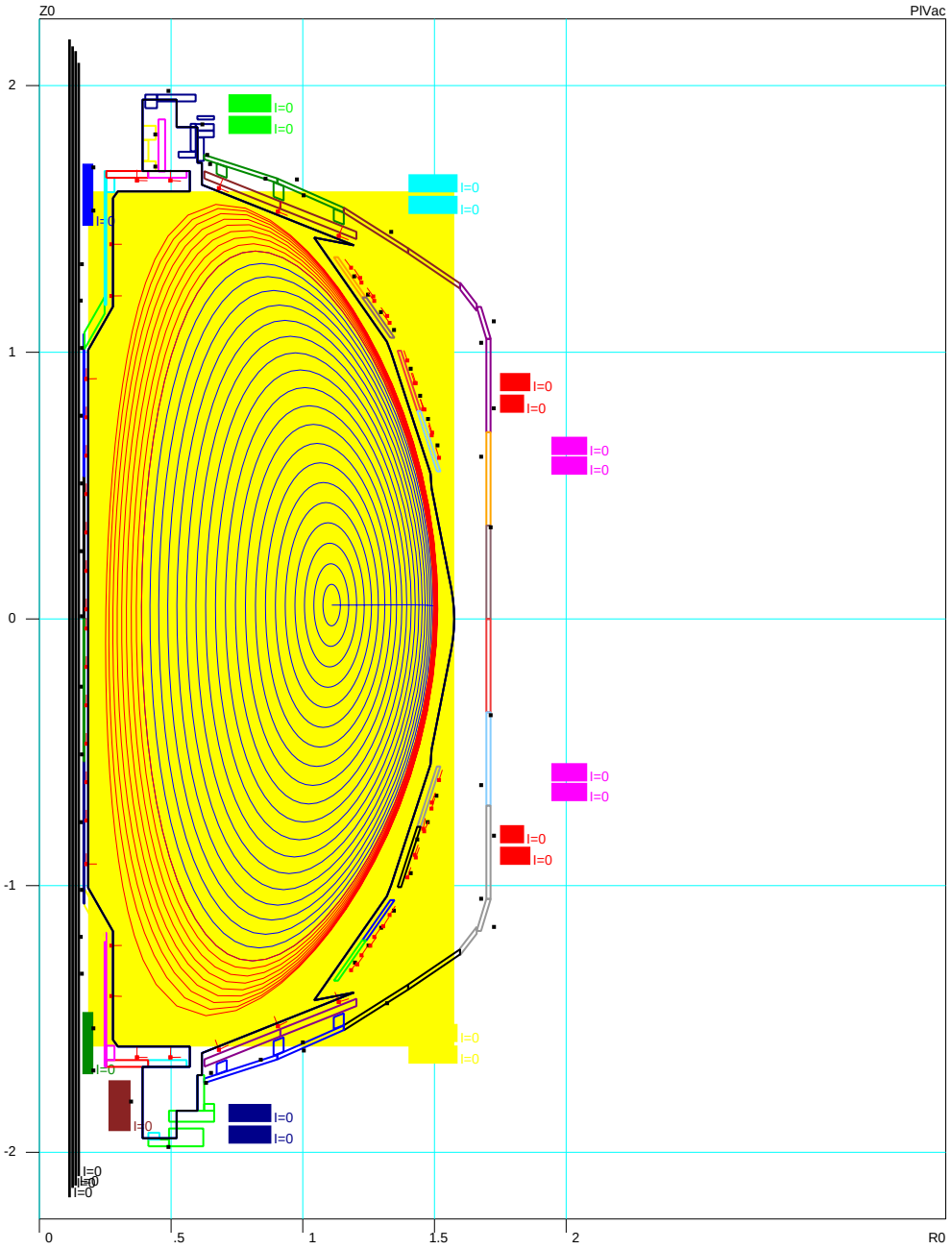

With $\beta \simeq 30\%$ the finite elements at the low field side of the plasma edge become narrower than the plot line.

EEC still works !

2.8 High-beta in NSTX with a separatrix

Small aspect ratio tokamak configuration: $R = 0.88$ ***m,*** $a = 0.65$ ***m***

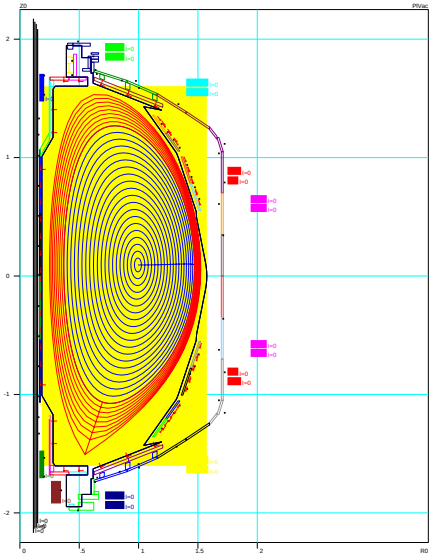

$\beta = 4\%$

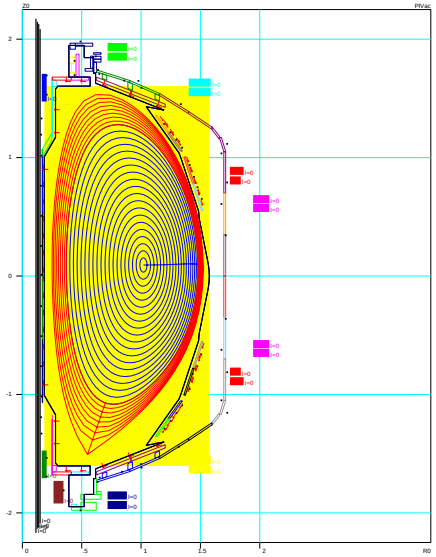

$\beta = 8\%$

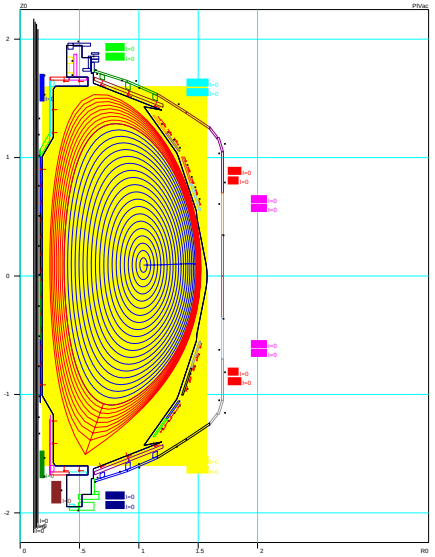

$\beta = 12\%$

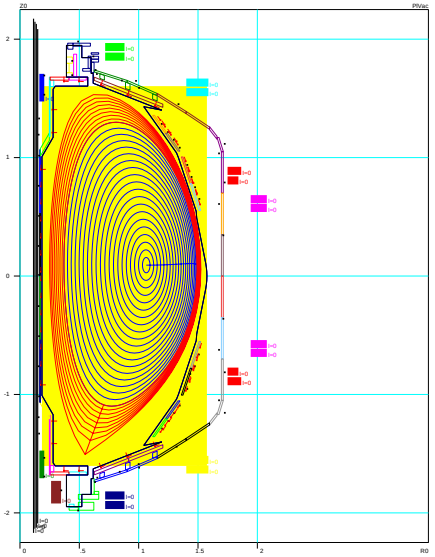

$\beta = 16\%$

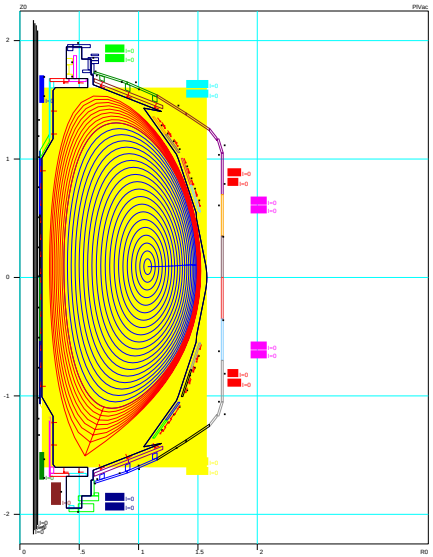

$\beta = 20\%$

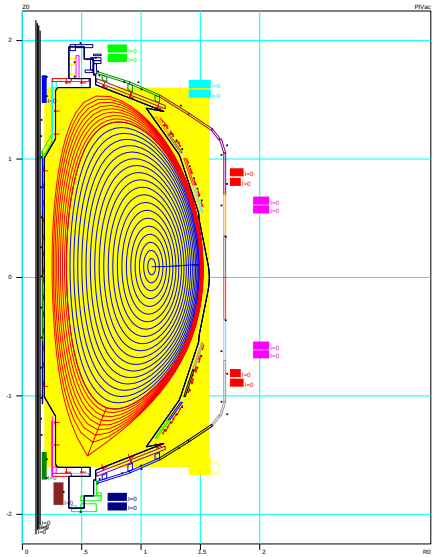

$\beta = 22\%$

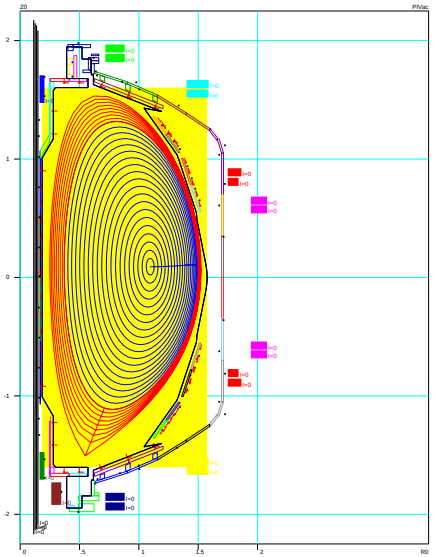

$\beta = 24\%$

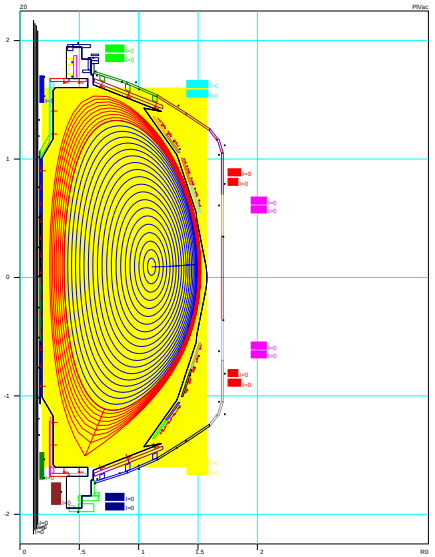

$\beta = 33\%$

2.9 Examples of ITER equilibria

Low triangularity case

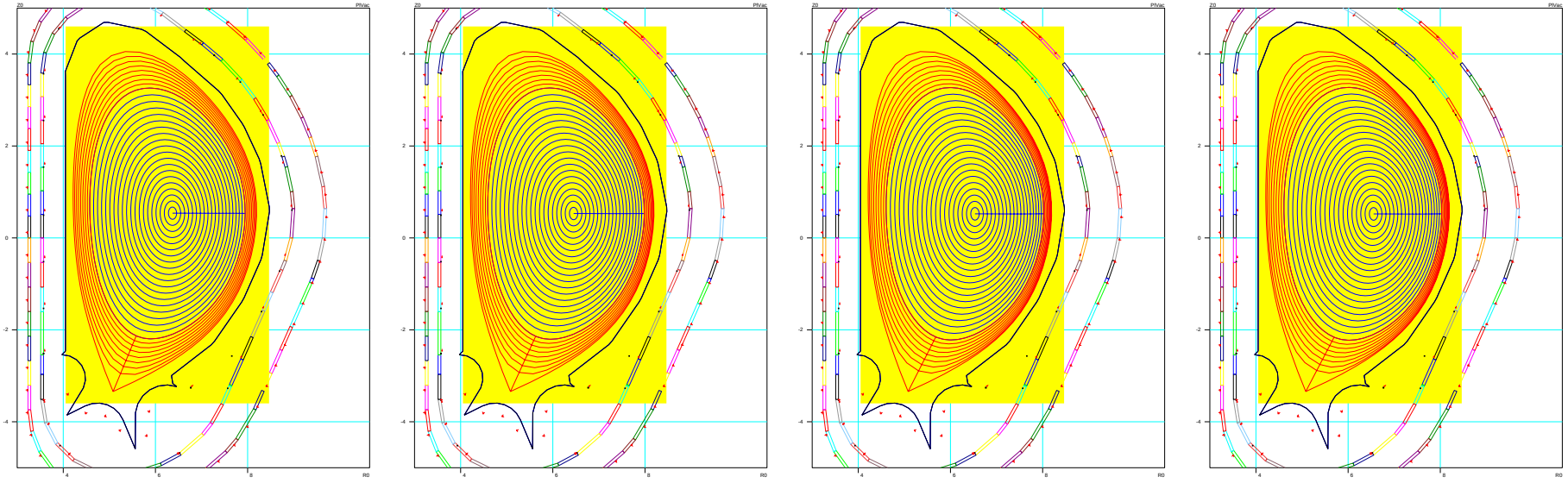

High triangularity case

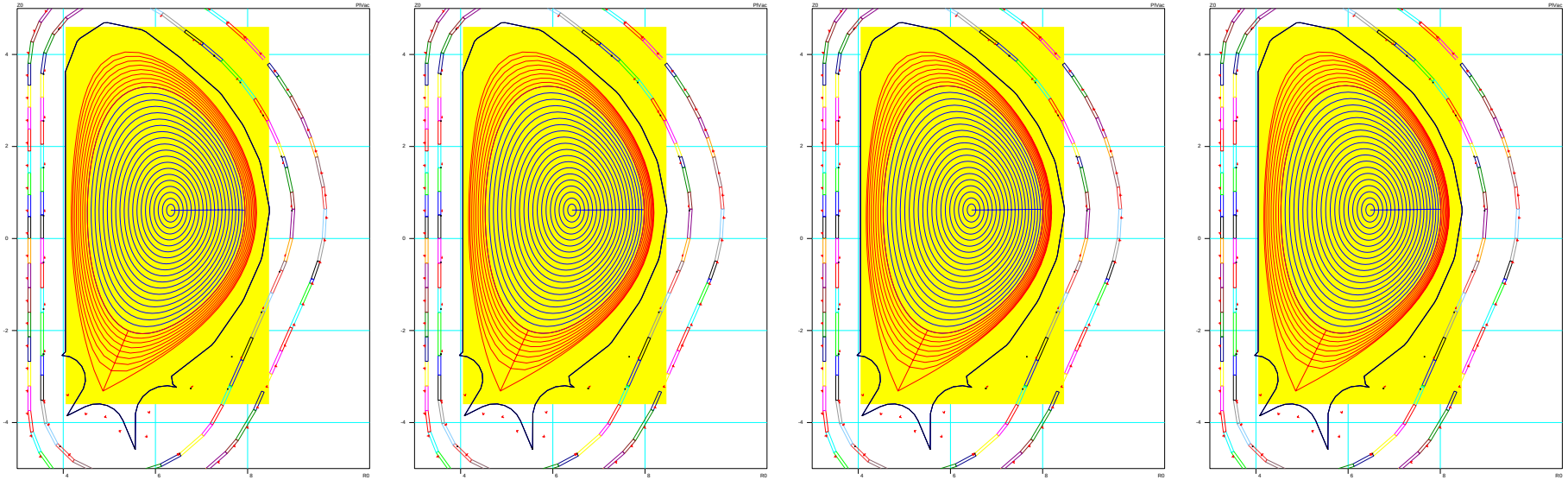

$\beta = 2\%$ $\beta = 4\%$ $\beta = 5\%$ $\beta = 6\%$

3 Summary

The ESC-EEC code system has been created for addressing major equilibrium problems

1. ***Several grid generators for Hermite finite elements are developed for plasma edge region in curvilinear coordinates;***
2. ***All combinations of Dirichlet and Neumann boundary conditions are implemented;***
3. ***Special matching conditions across finite elements at the X-point are implemented;***
4. ***Fast solver of tri-diagonal matrix equations was developed;***
5. ***The numerical scheme was validated against exact solutions;***
6. ***The core equilibrium code ESC was interfaced with EEC using***
   - ***(a) I/O files;***
   - ***(b) Sheared memory;***
   - ***(c) MPI;***
   - ***(d) Sockets.***

The architecture of ESC-EEC as two independent communicating codes addresses the difficult problem of code maintenance and their further unconflicting development.

ESC-EEC (+ASTRA) gives a practical approach to integration of numerical codes when people with different background contribute efficiently to the code system.